Biogeosciences Discuss., 12, 16645–16672, 2015
www.biogeosciences-discuss.net/12/16645/2015/
doi:10.5194/bgd-12-16645-2015

Biogeosciences Discussions
Open Access

Interactive effects of and light on growth rates and RUBISCO content of small and large centric diatoms

G. Li[1,2] and D. A. Campbell[1]

[1]Biology Department, Mount Allison University, Sackville, New Brunswick, E4L 1G7, Canada
[2]Key Laboratory of Tropical Marine Bio-resources and Ecology, South China Sea Institute of Oceanology, CAS, Guangzhou, 510301, China

Received: 24 September 2015 – Accepted: 28 September 2015 – Published: 16 October 2015

Correspondence to: D. A. Campbell (dcampbell@mta.ca)

Published by Copernicus Publications on behalf of the European Geosciences Union.

Abstract

Among marine phytoplankton groups, diatoms span the widest range of cell size, with resulting effects upon their nitrogen uptake, photosynthesis and growth responses to light. We grew two strains of marine centric diatoms, the small *Thalassiosira pseudonana* and the larger *T. punctigera* in high and low nitrogen media, across a range of growth light levels. Nitrogen and total proteins per cell decreased with increasing growth light in both species when grown under low nitrogen media. Surprisingly, low nitrogen increased the cellular allocation to RUBISCO and the rate of electron transport away from Photosystem II for the smaller diatom under low growth light, and for the larger diatom across the range of growth lights. Low nitrogen decreased the growth rate of the smaller diatom, particularly under higher light, but stimulated the growth rate of the larger diatom. Our results show that the high nitrogen in common growth media favours the growth rate of a small diatom but inhibits growth of a larger species.

1 Introduction

Nitrogen is critical for marine phytoplankton to build abundant cellular materials including proteins and nucleic acids to support their growth and cell division (Finkel et al., 2010; Li et al., 2015; Wu et al., 2014a). One of these nitrogen-rich materials, the Ribulose-1,5-bisphosphate Carboxylase Oxygenase (RUBISCO) protein is particularly important, because this bifunctional enzyme catalyzes the initial step of photosynthetic carbon reduction by combining CO_2 with Ribulose-1, 5-bisphosphate (RuBP) (Mizohata et al., 2002), fixing inorganic carbon to organic matter (Kroth, 2015). Nitrogen availability can affect the cellular content of RUBISCO with effects upon phytoplankton carbon assimilation (Wilhelm et al., 2006), particularly under N-limited conditions where RUBISCO has been suggested to act as an N reservoir (Falkowski et al., 1989). Available nitrogen is indeed considered as the proximal limiting factor for marine primary

BGD
12, 16645–16672, 2015

production (Gruber and Galloway, 2008; Moore et al., 2013) in much of the modern ocean.

Marine diatoms are the dominant group of phytoplankton (Wilhelm et al., 2006) in the modern ocean (Bowler et al., 2010) and account for approximately 20 % of global primary productivity (Field et al., 1998). Diatoms also span a wide size range across species from less than 2 to over 200 µm in equivalent spherical diameter, giving over eight orders of magnitude in cell volume (Beardall et al., 2009; Finkel et al., 2010). Diatom cell size affects many physiological processes, including light energy absorption (Finkel, 2001; Key et al., 2010), photosynthesis and respiration (López-Sandoval et al., 2014; Wu et al., 2014b), nutrient diffusion and uptake (Marañón et al., 2013; Raven, 1998; Raven and Kubler, 2002), and ultimately affects their growth (Marañón et al., 2013; Mei et al., 2011; Wu et al., 2014b).

Small phytoplankton cells have a higher surface area to volume ratio and can have lower nutrient requirements for growth (Finkel et al., 2010; Raven, 1998), thus they often dominate in nitrogen-limited and clear oceanic waters (Clark et al., 2013). Furthermore, pigment packaging in large phytoplankton can lead to a decline in light absorption per unit of pigment-protein complex (Clark et al., 2013; Finkel, 2001; Key et al., 2010) and a decrease in captured photons per unit of metabolic nitrogen invested into pigment protein complexes (Raven, 1984; Wu et al., 2014a) and the carbon assimilation per RUBSICO molecule (Wu et al., 2014a), again conferring advantages to smaller phytoplankton. The prevalence of larger phytoplankton cells in eutrophic and brackish coastal waters can be explained by enhanced resistance to predation (Ward et al., 2012), greater nutrient storage capacity (Grover, 2011), and lower metabolic costs to withstand and exploit fluctuating light because of lower susceptibility to photoinactivation of Photosystem II (Key et al., 2010). We found that under near-saturating growth light and nitrogen repletion larger diatoms invested more cellular nitrogen to RUBISCO than did smaller ones, to counter their lower achieved RUBISCO turnover rate (Wu et al., 2014a), a finding paralleled by increased allocations to RUBISCO in cold water diatoms where RUBISCO performance is kinetically limited (Losh et al., 2013;

BGD
12, 16645–16672, 2015

Young et al., 2015). To explain our finding of slower achieved RUBISCO turnover in larger diatoms (Wu et al., 2014a) we hypothesized that under nitrogen repletion large cells have luxury accumulation of RUBISCO protein, that in turn lowers their achieved performance per unit RUBISCO. To test this hypothesis, we grew two representative diatom strains; small *Thalassiosira pseudonana* ($\sim 40\,\mu m^3$) and large *T. punctigera* ($\sim 300\,000\,\mu m^3$) in chemostats across a range of growth light, in low nitrogen (LN) media to limit cellular luxury accumulation of RUBISCO protein, compared with cells grown in typical laboratory high nitrogen (HN) media. We determined the RUBISCO content across the species, nitrogen levels and growth light range, and analyzed in parallel how changing RUBISCO contents and turnover rate interact with changes in growth rates of the small and large diatoms.

2 Materials and methods

2.1 Culture protocol and growth rate

Two marine centric diatom strains *Thalassiosira pseudonana* (CCMP 1335) and *Thalassiosira punctigera* (CCAP 1085/19) were obtained from the Provasoli-Guillard National Center of Marine Phytoplankton and cultured in rectangular cuvettes (450 mL volume) of FMT-150 photobioreactors with two cm optical pathlength for illumination from a flat array of blue LED lights facing the rear face of the cuvette (Photon Systems Instruments, Drasov, Czech Republic) at 18 °C. We used two media for cultures: high nitrogen media (HN, $\sim 550\,\mu M\,NO_3^-$), enriched artificial seawater (EASW) (Berges et al., 2001) except with 54.5 µM Si and 0.82 µM Sr to limit precipitation during autoclaving; or low nitrogen media (LN, $\sim 55\,\mu M\,NO_3^-$), the same EASW except with one tenth of the nitrogen level of HN media, corrected with equal sodium bicarbonate to equivalent total alkalinity. We gently mixed the cultures with a curtain of bubbles emitted from four apertures across the cuvette bottom with outdoor fresh air that was filtered through a 0.2 µm micro-filter and bubbled through sterile distilled water for humidification before

BGD
12, 16645–16672, 2015

bubbling through the culture cuvette. We provided continuous growth light measured with a microspherical quantum sensor (US-SQS, Walz, Germany). The light levels in the culture vessels filled with media were set to 30, 180 and 380 µmol photons m^{-2} s^{-1} for *T. pseudonana* and to 30, 90 and 180 µmol photons m^{-2} s^{-1} for *T. punctigera*.

As described in detail for a previous project (Li and Campbell, 2013) we grew each experimental replicate culture from initial inoculation for 5–6 generations without dilution in batch mode to reach a cell density set-point for subsequent turbidostat mode, monitored continuously using the onboard fluorescence sensor in the bioreactors. We controlled the culture cell suspension density to $3.6 \pm 1.8 \times 10^5$ cells mL^{-1} for *T. pseudonana* and 650 ± 110 cells mL^{-1} for *T. punctigera*. When the fluorescence detector reached the set threshold the bioreactors activated a peristaltic pump to dilute the 450 mL culture with a 10 % volumetric addition of media delivered from a reservoir, which was continuously pre-bubbled with fresh air stream before adding to the cultures. Under these conditions the cells depleted the nitrogen concentration within the culture volume to ~ 500 µM in HN and to < 10 µM NO_3^- in LN media. 3.5 L of media in the reservoir supported ~ 9.5 cellular generations of turbidostat growth for each replicate culture under the set conditions of light and nitrogen, before we harvested for physiological and biochemical analyses. Depending upon the achieved growth rate, which varied with growth light, nitrogen and species, the temporal duration of each turbidostat run ranged from 160 to 200 h. We calculated the growth rate for a given culture replicate by fitting the increase in OD_{680}, measured with the onboard detector in the bioreactors, with time with an exponential growth function for each turbidostat cycle of a 10 % increase in cell density followed by dilution once the culture reached the set threshold. We then averaged the exponential rates from the final 10 cycles of turbidostat dilution to estimate the growth rate for each replicate (Li and Campbell, 2013). We grew 3 or 4 separate replicate cultures of each species under each combination of light and media, for a total of 39 separate turbidostat runs.

BGD
12, 16645–16672, 2015

2.2 Chlorophyll fluorescence measurements

At the end of each growth period we took out 2 mL culture from each turbidostat cuvette, dark-adapted for 5 min within a cuvette with temperature control (18 °C) and measured the chlorophyll fluorescence with a fluorometer (PSI FL 3500, Photon Systems Instruments, Czech Republic) using the Fast Repetition Rate fluorescence technique (Kolber et al., 1998). A series of 40 × 1.2 µs flashlets of blue light were applied over 128 µs (455 nm; ~ 100 000 µmol photons $m^{-2} s^{-1}$) were provided to progressively close PSII reaction centers. The resulting FRR induction curve was analyzed with the PSIWORX script for MATLAB (Audrey Barnett, www.sourceforge.net), to define F_0, the base line fluorescence in dark-adapted cells, F_M, the maximal fluorescence with all PSII closed and σ_{PSII} (10^{-20} m^2 quanta^{-1}), the effective absorbance cross section serving PSII photochemistry in the dark-adapted cells. After a 2 s dark period we applied a second FRR induction. We then activated an actinic blue light to the growth light level for 2 min; again, we captured the FRR induction curves to extract parameters in illuminated cells, to define F_S, the fluorescence in light acclimated state, $F_{M'}$, the maximal fluorescence with all PSII closed and $\sigma_{PSII'}$ (10^{-20} m^2 quanta^{-1}), the effective absorbance cross section serving PSII photochemistry in the light acclimated state. We then applied an FRR induction after a 2 s dark period again, to allow re-opening of closed PSII centers. There was a slight drop in the level of fluorescence from F_S to $F_{0'2s}$, the baseline fluorescence with all PSII open but still in light acclimated state.

We calculated the maximal photochemical yield in dark-adapted cells as:

$$F_V/F_M = (F_M - F_0)/F_M$$

We also used the magnitude of any increase from $F_{M'}$ to $F_{M'2s}$ to apply a proportional correction to $F_{0'2s}$ to estimate the actual level of $F_{0'}$ under illumination:

$$F_{0'} = F_{0'2s} \times \left\{1 - \left[\left(F_{M'2s} - F_{M'}\right)/F_{M'2s}\right]\right\}$$

BGD
12, 16645–16672, 2015

We estimated the electron transport rate away from PSII following (Huot and Babin, 2010) as:

PSII electron transport = $\sigma_{PSII'} \times I \times q_P$,

where, $\sigma_{PSII'}$ (10^{-20} $m^2 quanta^{-1}$) is the effective absorbance cross section serving PSII photochemistry at growth light I (photons A^{-2} s^{-1}), and q_P, $(F_{M'} - F_S)/(F_{M'} - F_{0'})$ is the proportion of PSII instantaneously open and ready to perform photochemistry under light I. We also used the FRR data and PSIWORX-MATLAB to extract the life times for fluorescence relaxation after a saturating flash, τ_1 and τ_2 to measure the down-stream metabolic capacity to carry electrons away from PSII (Kolber et al., 1998).

2.3 Cell density, protein and Chlorophyll *a* measurements

At the end of each turbidostat growth period we took duplicate 2 mL culture samples, fixed in Lugol's acid solution and measured the cell suspension density with a Coulter Z2 counter (Beckman Instruments, Florida, US) for *T. pseudonana* and with a Sedgwick Rafter chamber under a microscope for *T. punctigera*. Simultaneously, we vacuum-filtered 50 mL of culture sample onto a binder-free Whatman GF/F glass fiber filter (25 mm in diameter), which was immediately flash frozen in liquid nitrogen and stored at −80 °C until later analyses of protein and chlorophyll.

Immunoquantitations of specific protein subunits from total protein extracts followed (Brown et al., 2008). Briefly, total protein was extracted from the frozen filters using the MPBio FastPrep®-24 with bead lysing matrix **D** (SKU 116 913 050) and 450 µL of 1X denaturing extraction buffer (0.1375 mol L^{-1} TRIS buffer, 0.075 mol L^{-1} LDS, 1.075 mol L^{-1} glycerol, 0.5 mmol L^{-1} EDTA, 0.1 mg mL^{-1} Pefabloc) (Brown et al., 2008) for three cycles of 60 s at 6.5 m s^{-1}. Total protein in the extracts was determined using Bio-Rad DC protein assay kit (500–0116) with known bovine gamma globulin standards. Samples containing 0.5 µg of total protein were loaded on 4 to 12 % acrylamideprecast NuPAGE gels (Invitrogen) to determine RUBISCO large subunit (RbcL)

BGD
12, 16645–16672, 2015

and Photosystem II PsbA subunit, run in parallel with a range of RbcL standard (Agrisera, www.agrisera.se, AS01 017S) and PsbA standard (Agrisera, www.agrisera.se, AS01 016S) to establish a standard curve. Electrophoresis was run for 25 min at 200 V and the proteins were transferred to a polyvinylide fluoride (PVDF) membrane for 60 min at 30 V for RbcL and 20 V for PsbA. After the membrane blocking, a primary antibody (Agrisera, AS03 037 and AS05 084, 1 : 20 000 dilution) was applied, followed by an anti-rabbit secondary antibody coupled with horseradish peroxidase (Agrisera, AS09 602, 1 : 20 000). The membranes were then developed by chemoluminescence using ECL Advance (GE Biosciences) and imaged under a CCD imager (BioRadVersaDoc 4000MP). Finally, the RbcL and PsbA protein quantitation was determined by fitting the sample signal values to the protein standard curves, taking care that all sample signals fell within the range of protein standard curve and that no band signals were saturated (Brown et al., 2008).

For Chlorophyll *a* (Chl *a*) measurement, 50 µL of protein extract was added to 450 µL 90 % acetone (*v*/*v*) saturated with magnesium carbonate; after 15 min extraction in the dark at 4 °C and 2 min centrifugation (13 000 g), we measured the absorbance of the supernatant at 664, 630 and 750 nm using a UV/VIS photospectrometer (UV-1800, Shimadzu, Japan). The µg Chl *a* mL^{-1} extract was estimated following (Jeffrey and Humphrey, 1975):

$$[\text{Chl } a] = 11.47 \times (A_{664} - A_{750}) - 0.4 \times (A_{630} - A_{750})$$

2.4 Carbon and nitrogen analyses

At the end of each turbidostat growth period we filtered 50 mL of culture onto a precombusted (5 h, 450 °C) Whatman GF/F glass fiber filter (13 mm in diameter), rinsed with 10 mL of 50 mmol HCl L^{-1} to remove inorganic carbon, dried at 55 °C for 12 h and stored in a desiccator for later analyses. Contents of carbon and nitrogen were measured with a Vario EL III Elemental Analyzer (Elementar, Hanau, Germany).

BGD
12, 16645–16672, 2015

2.5 Data analysis

The response of growth rate to culture growth light was fitted with either linear regressions or with the equation of (Eilers and Peeters, 1988):

$$\mu = I/(a \times I^2 + b \times I + c)$$

where: μ is growth rate (d^{-1}) at the particular light level; I is the growth light (µmol photons $m^{-2} s^{-1}$) and a, b and c are fitted parameters.

$$\mu_{max} = 1/(b + 2\sqrt{a \times c})$$

We used ANOVA with Bonferroni post-tests (Prism 5, Graphpad Software) and comparisons of linear and non-linear curve fits to detect significant differences between cultures from LN and HN media of each species; and we used t test to detect the significant differences between LN and HN under each growth light.

3 Results

The cell growth rate of *Thalassiosira pseudonana* growing in HN media increased with growth light from low (~ 30 µmol photons $m^{-2} s^{-1}$) to moderate levels (~ 180 µmol photons $m^{-2} s^{-1}$) reaching a fitted μ_{max} of 1.5 d^{-1} but then decreased under higher light (~ 380 µmol photons $m^{-2} s^{-1}$) (Fig. 1a). The growth rate in LN media was lower than in HN media, and linearly decreased from 0.92 to 0.59 d^{-1} with increasing growth light from ~ 30 to ~ 380 µmol photons $m^{-2} s^{-1}$ (Fig. 1a), thus under LN 30 µmol photons $m^{-2} s^{-1}$ was already growth-saturating for *Thalassiosira pseudonana*, albeit at a lower μ_{max} than under HN. The growth rate of *T. punctigera* in HN media was much slower than *T. pseudonana* but showed a qualitatively similar light response pattern, increasing with growth light from ~ 30 to ~ 90 µmol photons $m^{-2} s^{-1}$ with a fitted μ_{max} of 0.39 d^{-1} but then decreasing under ~ 180 µmol photons $m^{-2} s^{-1}$ (Fig. 1b). The

BGD
12, 16645–16672, 2015

growth rate of *T. punctigera* in LN media was significantly higher than in HN media, particularly under the lower growth light; it decreased linearly from 0.66 to 0.54 d^{-1} with increasing growth light from 30 to 180 µmol photons m^{-2} s^{-1} (Fig. 1b), thus again for *T. punctigera* under LN 30 µmol photons m^{-2} s^{-1} was already growth-saturating, with a μ_{max} higher under LN than under HN. Note that there were small variations in the light sources among our three bioreactor units, so we plotted the specific growth rates and other parameters vs. the actual light level applied to a given culture condition replicate, resulting in small offsets in data points along the *x* axes of plots, which slightly improved the statistical power of our curve fitting.

Cellular carbon content for *T. pseudonana* and for *T. punctigera* showed no apparent trends with growth light nor with media nitrogen level (Table 1). Under high nitrogen *T. pseudonana* total protein content ranged from 4.61 to 4.88 pg $cell^{-1}$, but under low nitrogen there was a surprising higher pg protein $cell^{-1}$ under the lowest growth light (Table 1). *T. punctigera* showed scatter among replicates in pg protein $cell^{-1}$ with a weak downward trend with increasing light, but again showed higher pg protein $cell^{-1}$ in low nitrogen media (Table 1).

Cellular nitrogen content in *T. pseudonana* decreased from 1.55 to 1.27 pg $cell^{-1}$ as growth light increased, with no statistically significant effect of media nitrogen level (Fig. 2a). The N content in *T. punctigera* showed a similar light response pattern as *T. pseudonana* for the cultures grown in LN media where the N content decreased from 1085 to 896 pg $cell^{-1}$ with increasing light. The low N media lowered *T. punctigera* cellular N content across all growth light conditions (Fig. 2b). We estimated the fraction of cellular nitrogen allocated to Chlorophyll *a* (Chl *a*, Table 1), to Photosystem II (extrapolated from molar contents of the PsbA subunit, Table 1) and to RUBISCO protein (extrapolated from molar contents of the RbcL subunit, Table 1) as in (Li et al., 2015). The molar fraction of Chl *a* N to total cellular N (Chl *a* N : total N) in *T. pseudonana* decreased from 0.011 to 0.0046 with increasing growth light, with no significant effect of media N (Fig. 2c). Under high nitrogen the Chl *a* N : total N in *T. punctigera* decreased from 0.0048 to 0.0027, and was significantly increased by lower media N

BGD
12, 16645–16672, 2015

across the growth lights (Fig. 2d). Under high nitrogen PSII N : total N in *T. pseudonana* was ~ 0.013 across the light levels; low media N significantly increased the PSII N : total N to 0.0025 at lowest growth light (Fig. 2e). The PSII N : total N in *T. punctigera* varied from 0.014 to 0.0077, with scatter among replicates but no apparent trends with growth light nor with media nitrogen level (Fig. 2f). The molar fraction of N allocated to RUBISCO relative to total cellular N under high nitrogen slightly increased from 0.061 to 0.086 for *T. pseudonana* as growth light increased and varied from 0.019 to 0.034 with no clear trends for *T. punctigera.* (Fig. 2g and h). For *T. pseudonana* under low growth light, and for *T. punctigera* across the growth lights growth in low nitrogen media had a surprising effect of increasing the cellular content of RUBISCO, with parallel effects upon cellular protein content. Thus our initial goal of using lower media N to restrict the cellular allocation of N to RUBISCO failed. Our results do show that in *T. punctigera* the RUBISCO content under HN does not likely represent luxury accumulation, because the fractional allocation of N to RUBISCO increased further under LN media.

Maximum photochemical quantum yield of Photosystem II (F_V/F_M) ranged from 0.57 to 0.59 in *T. pseudonana* with no significant effect of growth light, nor nitrogen level (Fig. 3a). The F_V/F_M of *T. punctigera* decreased from 0.44 to 0.32 with increasing growth light in high nitrogen media, but was higher in low nitrogen media (Fig. 3b) showing that the high nitrogen resulted in inhibition of PSII function, even under low growth light in *T. punctigera.* The functional absorption cross-section for PSII photochemistry (σ_{PSII}) decreased from 350 to 151×10^{-20} m^2 quanta^{-1} with increasing growth light in *T. pseudonana,* with no significant nitrogen effects (Fig. 3c) in parallel with the pattern for Chl *a* per cell (Table 1; Fig. S1 in the Supplement), while the σ_{PSII} for *T. punctigera* ranged from 246 to 168×10^{-20} m^2 quanta^{-1} and showed no effects of growth light nor nitrogen level (Fig. 3d). PSII electron transfer rate (ETR) for *T. pseudonana* increased from 74 to 287 e^- $PSII^{-1}$ s^{-1} with increasing growth light from 30 to 380 µmol photons m^{-2} s^{-1} with no significant nitrogen effect (Fig. 3e). The PSII ETR for *T. punctigera* increased with growth light in high nitrogen media but increased more under LN media (Fig. 3f) because of the higher PSII photochemistry under LN (Fig. 3b).

BGD
12, 16645–16672, 2015

The rate constant for ($1/\tau_1$, s^{-1}) for PSII re-opening after saturating flash ranged from 175 to 230 s^{-1} in *T. pseudonana* with no significant effect of growth light, nor of nitrogen level (Fig. 3g). The $1/\tau_1$ for *T. punctigera* varied from 117 to 121 s^{-1} in HN media, slower than in LN media (Fig. 3h), indicating the high media N source inhibits the rate of electron transport away from PSII (Kolber et al., 1998). The $1/\tau_1$ of *T. punctigera* accelerated from 158 to 197 s^{-1} with increasing growth light in LN media, but not in HN media, making electron transport away from PSII faster in LN media at higher light (Fig. 3h).

When we plotted growth rate (μ) against the molar ratio of nitrogen allocation to RUBISCO relative to total cellular nitrogen, a common, saturating, fit (Eilers and Peeters, 1988) explained the variation for both *T. pseudonana* (LN) and *T. punctigera* (LN, HN), with growth rate reaching half saturation at a RUBISCO N : total N of 0.058. *T. pseudonana* grown in HN media, however, fell well above this pooled fitted curve (Fig. 4a). Similarly, the apparent RUBISCO turnover rate of *T. pseudonana* from LN media and *T. punctigera* from LN and HN media showed a negative linear correlation with RUBISCO N : total N; but again *T. pseudonana* in HN media fell above the curve (Fig. 5b). $1/\tau_1$ the rate constant for electron transport away from PSII, shows a saturating pattern when plotted vs. RUBISCO N : total N, for all treatments (Fig. 5a and c) (Zorz et al., 2015). On a plot of of μ and $1/\tau_1$ (Fig. 6) all treatments fell on a common rising linear trend, again except for *T. pseudonana* in HN media, which achieved higher growth at a given $1/\tau_1$ (Fig. 6).

4 Discussion

In an earlier study (Wu et al., 2014a) we found that compared to small diatoms, larger diatoms increase their allocation of cellular nitrogen to RUBISCO when growing under nitrogen rich media and high light, a finding consistent with our findings herein (Fig. 2g and h, closed symbols, high growth light). In this study we sought to test whether this

BGD
12, 16645–16672, 2015

RUBISCO allocation in larger cells represented a luxury accumulation of excess that could account for their low apparent C RbcL^{-1} s^{-1}. We therefore grew a small and large diatom under high and low nitrogen levels. We achieved the expected growth limitation by low nitrogen in the smaller diatom, which nevertheless maintained its RbcL content (Table 1) and thus suffered a decrease in achieved C RbcL^{-1} s^{-1} (Fig. 4b, closed vs. open squares) under low nitrogen. In contrast, at the lowest media nitrogen level ($< 10\,\mu M\,NO_3^-$) that we could reliably apply the larger diatom enjoyed increased growth rates, particularly under lower light (Fig. 1b). Therefore we failed to achieve a growth-limiting N concentration for *T. punctigera*. Indeed, in our low nitrogen media *T. punctigera* actually increased its cellular allocation of nitrogen to RUBISCO (Table 1), while in parallel achieving comparable C Rbcl^{-1} s^{-1} (Fig. 4b) as under HN. Thus, the low performance of C Rbcl^{-1} s^{-1} in our larger diatoms in our earlier study was not attributable to luxury accumulation of excess RUBISCO, but rather in part to a limitation on their growth rates under typical laboratory media concentrations of NO_3^-.

Nitrogen is a major material to build up cells; therefore, a low media N level is usually believed to limit phytoplankton growth (Li and Gao, 2014; Mei et al., 2011; Moore et al., 2013) as found here for *T. pseudonana* (Fig. 1a). This situation is however species-specific since lower nitrogen inhibited the growth of the smaller *T. pseudonana* but stimulated the growth of the larger *T. punctigera* (Fig. 1). Mechanistically, there are two main strategies for phytoplankton to maintain growth rate when the growth environment is not favorable; to increase the abundance of rate limiting enzymes or to increase the achieved enzymatic rates (activities), as shown in particular by studies of the enzyme responsible for carbon fixation, RUBISCO (Feller and Gerday, 2003; Young et al., 2015). In this view-point, phytoplankton could allocate more of their cellular N to growth rate-limiting enzymes, as for example RUBISCO, to maintain their growth when the media N source is low, consistent with our results for *T. pseudonana* grown at low growth light (Fig. 2g) and *T. punctigera* grown across three light levels (Fig. 2h). Meanwhile, the lower N source greatly decreased the activities of RUBISCO in the small *T. pseudonana*

BGD
12, 16645–16672, 2015

but not in the larger *T. punctigera* (Fig. 4b), showing differential effects of lower N source on the amount and achieved activity of RUBISCO in small and large diatoms.

Enzymes, including RUBISCO, have thermal optimums (Feller and Gerday, 2003). Young et al. (2015) found that to compensate for slow enzymatic rates at low temperatures, Antarctic diatoms up-regulated both RUBISCO allocation and other cellular proteins needed for C fixation, to maintain productivity to support the intense spring/summer blooms in high-latitude waters, despite water temperatures close to freezing. Our results are consistent since higher RUBISCO abundance supported higher growth rates of both *T. pseudonana* and *T. punctigera*, but the relation shifted differentially for each species under high or low N source media (Fig. 4a), with *T. pseudonana* able to upregulate achieved RUBISCO performance under high N.

In recent decades, marine nitrogen concentration has increased globally, in particular in coastal waters or estuaries, such as in Hong Kong waters where nitrate reaches 40 µM in summer (Xu et al., 2012), in the Danube River estuary, northwestern Black Sea where nitrate reached 50 µM (Möbius and Dähnke, 2015) and in the Jiulong River estuary, northern South China Sea where nitrate reached over 80 µM (Li et al., 2011). According to our findings (Fig. 1b), such nitrate levels are far above the optimal growth nitrogen levels for large *T. punctigera*, and are sufficient to inhibit its growth. In contrast yet higher nitrate levels can further stimulate the growth of small *T. pseudonana* (Fig. 1a). Therefore, the different stimulation and inhibition effects of media N source on larger and smaller cells growth could have important implications for ecosystem phytoplankton community changes due to the worldwide increasing marine eutrophications.

5 Summary

We grew small and large marine centric diatoms, *T. pseudonana* and *T. punctigera*, in high and low nitrogen media, across a range of growth light. Surprisingly growth limiting low nitrogen did not significantly lower cellular N content in the small *T. pseudonana*. In contrast the same low nitrogen level stimulated faster growth in the larger *T. punctig-*

BGD
12, 16645–16672, 2015

era, which actually increased in cellular nitrogen content under low nitrogen media. Furthermore, we found low media nitrogen increased the cellular RUBISCO content of the smaller cells at limiting light, and of the larger cells across the growth light range. These unexpected effects upon RUBISCO under low nitrogen altered the growth responses to light in both strains.

The Supplement related to this article is available online at doi:10.5194/bgd-12-16645-2015-supplement.

Acknowledgements. Jessica Grant-Burt did cell count determinations for *Thalassiosira punctigera*. Miranda Corkum and Ina Benner assisted with the CN analyses. This work was supported by the Canada Research Chairs program (DC) using equipment supported by the Canada Foundation for Innovation and the New Brunswick Innovation Foundation. G. Li was supported by National Natural Science Foundation of China (41 206 132) and Natural Science Foundation of Guangdong Province, China (2015A030 313 826).

References

Beardall, J., Allen, D., Bragg, J., Finkel, Z. V., Flynn, K. J., Quigg, A., Rees, T. A. V., Richardson, A., and Raven, J. A.: Allometry and stoichiometry of unicellular, colonial and multicellular phytoplankton, New Phytol., 181, 295–309, doi:10.1111/j.1469-8137.2008.02660.x, 2009.

Berges, J. A., Franklin, D. J., and Harrison, P. J.: Evolution of an artificial seawater medium: improvements in enriched seawater, artificial water over the last two decades, J. Phycol., 37, 1138–1145, doi:10.1046/j.1529-8817.2001.01052.x, 2001.

Bowler, C., Vardi, A., and Allen, A. E.: Oceanographic and biogeochemical insights from diatom genomes, Annu. Rev. Mar. Sci., 2, 333–365, doi:10.1146/annurev-marine-120308-081051, 2010.

Brown, C., MacKinnon, J., Cockshutt, A., Villareal, T., and Campbell, D.: Flux capacities and acclimation costs in *Trichodesmium* from the Gulf of Mexico, Mar. Biol., 154, 413–422, 2008.

BGD
12, 16645–16672, 2015

Clark, J. R., Lenton, T. M., Williams, H. T. P., and Daines, S. J.: Environmental selection and resource allocation determine spatial patterns in picophytoplankton cell size, Limnol. Oceanogr., 58, 1008–1022, doi:10.4319/lo.2013.58.3.1008, 2013.

Eilers, P. H. C. and Peeters, J. C. H.: A model for the relationship between light intensity and the rate of photosynthesis in phytoplankton, Ecol. Model., 42, 199–215, doi:10.1016/0304-3800(88)90057-9, 1988.

Falkowski, P. G., Sukenik, A., and Herzig, R.: Nitrogen limitation in *Isochrysis galbana*, II. Relative abundance of chloroplast proteins., J. Phycol., 25, 471–478, doi:10.1111/j.1529-8817.1989.tb00252.x, 1989.

Feller, G. and Gerday, C.: Psychrophilic enzymes: hot topics in cold adaptation, Nat. Rev. Microbiol., 1, 200–208, doi:10.1038/nrmicro773, 2003.

Field, C. B., Behrenfeld, M. J., Randerson, J. T., and Falkowski, P.: Primary production of the biosphere: integrating terrestrial and oceanic components, Science, 281, 237–240, doi:10.1126/science.281.5374.237, 1998.

Finkel, Z. V.: Light absorption and size scaling of light-limited metabolism in marine diatoms, Limnol. Oceanogr., 46, 86–94, doi:10.4319/lo.2001.46.1.0086, 2001.

Finkel, Z. V., Beardall, J., Flynn, K. J., Quigg, A., Rees, T. A. V., and Raven, J. A.: Phytoplankton in a changing world: cell size and elemental stoichiometry, J. Plankton Res., 32, 119–137, doi:10.1093/plankt/fbp098, 2010.

Grover, J. P.: Resource storage and competition with spatial and temporal variation in resource availability, Am. Nat., 178, E124–E148, doi:10.1086/662163, 2011.

Gruber, N. and Galloway, J. N.: An Earth-system perspective of the global nitrogen cycle, Nature, 451, 293–296, doi:10.1038/nature06592, 2008.

Huot, Y. and Babin, M.: Overview of fluorescence protocols: theory, basic concepts, and practice, in: Chlorophyll *a* Fluorescence in Aquatic Sciences: Methods and Applications, edited by: Suggett, D. J., Prášil, O., and Borowitzka, M. A., Springer Netherlands, Dordrecht, 31–74, available at: http://www.springerlink.com/index/10.1007/978-90-481-9268-7_3 (last access: 29 October 2012), 2010.

Jeffrey, S. and Humphrey, G.: New spectrophotometric equations for determining chlorophylls a1, b1, c1 and c2 in higher plants, algae and natural phytoplankton, Biochem. Physiol. Pfl., 167, 191–194, 1975.

BGD
12, 16645–16672, 2015

Key, T., McCarthy, A., Campbell, D. A., Six, C., Roy, S., and Finkel, Z. V.: Cell size trade-offs govern light exploitation strategies in marine phytoplankton, Environ. Microbiol., 12, 95–104, doi:10.1111/j.1462-2920.2009.02046.x, 2010.

Kolber, Z. S., Prášil, O., and Falkowski, P. G.: Measurements of variable chlorophyll fluorescence using fast repetition rate techniques: defining methodology and experimental protocols, BBA-Bioenergetics, 1367, 88–106, doi:10.1016/S0005-2728(98)00135-2, 1998.

Kroth, P. G.: The biodiversity of carbon assimilation, J. Plant Physiol., 172, 76–81, doi:10.1016/j.jplph.2014.07.021, 2015.

Li, G. and Campbell, D. A.: Rising CO_2 interacts with growth light and growth rate to alter photosystem II photoinactivation of the coastal diatom *Thalassiosira pseudonana*, PLoS ONE, 8, e55562, doi:10.1371/journal.pone.0055562, 2013.

Li, G. and Gao, K.: Effects of solar UV radiation on photosynthetic performance of the diatom Skeletonema costatum grown under nitrate limited condition, ALGAE, 29, 27–34, doi:10.4490/algae.2014.29.1.027, 2014.

Li, G., Gao, K., Yuan, D., Zheng, Y., and Yang, G.: Relationship of photosynthetic carbon fixation with environmental changes in the Jiulong River estuary of the South China Sea, with special reference to the effects of solar UV radiation, Mar. Pollut. Bull., 62, 1852–1858, doi:10.1016/j.marpolbul.2011.02.050, 2011.

Li, G., Brown, C. M., Jeans, J., Donaher, N., McCarthy, A., and Campbell, D. A.: The nitrogen costs of photosynthesis in a diatom under current and future pCO_2, New Phytol., 205, 533–543, doi:10.1111/nph.13037, 2015.

López-Sandoval, D. C., Rodríguez-Ramos, T., Cermeño, P., Sobrino, C., and Marañón, E.: Photosynthesis and respiration in marine phytoplankton: relationship with cell size, taxonomic affiliation, and growth phase, J. Exp. Mar. Biol. Ecol., 457, 151–159, doi:10.1016/j.jembe.2014.04.013, 2014.

Losh, J. L., Young, J. N., and Morel, F. M. M.: Rubisco is a small fraction of total protein in marine phytoplankton, New Phytol., 198, 52–58, doi:10.1111/nph.12143, 2013.

Marañón, E., Cermeño, P., López-Sandoval, D. C., Rodríguez-Ramos, T., Sobrino, C., Huete-Ortega, M., Blanco, J. M., and Rodríguez, J.: Unimodal size scaling of phytoplankton growth and the size dependence of nutrient uptake and use, edited by G. Fussmann, Ecol. Lett., 16, 371–379, doi:10.1111/ele.12052, 2013.

BGD
12, 16645–16672, 2015

Mei, Z., Finkel, Z., and Irwin, A.: Phytoplankton growth allometry and size-dependent C : N stoichiometry revealed by a variable quota model, Mar. Ecol.-Prog. Ser., 434, 29–43, doi:10.3354/meps09149, 2011.

Mizohata, E., Matsumura, H., Okano, Y., Kumei, M., Takuma, H., Onodera, J., Kato, K., Shibata, N., Inoue, T., Yokota, A., and Kai, Y.: Crystal structure of activated ribulose-1,5-bisphosphate carboxylase/oxygenase from green alga Chlamydomonas reinhardtii complexed with 2-carboxyarabinitol-1,5-bisphosphate, J. Mol. Biol., 316, 679–691, doi:10.1006/jmbi.2001.5381, 2002.

Möbius, J. and Dähnke, K.: Nitrate drawdown and its unexpected isotope effect in the Danube estuarine transition zone: N isotope dynamics in the Danube Delta, Limnol. Oceanogr., 60, 1008–1019, doi:10.1002/lno.10068, 2015.

Moore, C. M., Mills, M. M., Arrigo, K. R., Berman-Frank, I., Bopp, L., Boyd, P. W., Galbraith, E. D., Geider, R. J., Guieu, C., Jaccard, S. L., Jickells, T. D., La Roche, J., Lenton, T. M., Mahowald, N. M., Marañón, E., Marinov, I., Moore, J. K., Nakatsuka, T., Oschlies, A., Saito, M. A., Thingstad, T. F., Tsuda, A., and Ulloa, O.: Processes and patterns of oceanic nutrient limitation, Nat. Geosci., 6, 701–710, doi:10.1038/ngeo1765, 2013.

Peeters, J. C. H. and Eilers, P.: The relationship between light intensity and photosynthesis – a simple mathematical model, Hydrobiol. Bull., 12, 134–136, doi:10.1007/BF02260714, 1978.

Raven, J. A.: A cost-benefit analysis of photon absorption by photosynthetic unicells, New Phytol., 98, 593–625, doi:10.1111/j.1469-8137.1984.tb04152.x, 1984.

Raven, J. A.: The twelfth Tansley Lecture, small is beautiful: the picophytoplankton, Funct. Ecol., 12, 503–513, doi:10.1046/j.1365-2435.1998.00233.x, 1998.

Raven, J. A. and Kubler, J. E.: New light on the scaling of metabolic rate with the size of algae, J. Phycol., 38, 11–16, doi:10.1046/j.1529-8817.2002.01125.x, 2002.

Ward, B. A., Dutkiewicz, S., Jahn, O., and Follows, M. J.: A size-structured food-web model for the global ocean, Limnol. Oceanogr., 57, 1877–1891, doi:10.4319/lo.2012.57.6.1877, 2012.

Wilhelm, C., Büchel, C., Fisahn, J., Goss, R., Jakob, T., LaRoche, J., Lavaud, J., Lohr, M., Riebesell, U., Stehfest, K., Valentin, K., and Kroth, P. G.: The regulation of carbon and nutrient assimilation in diatoms is significantly different from green algae, Protist, 157, 91–124, doi:10.1016/j.protis.2006.02.003, 2006.

BGD
12, 16645–16672, 2015

Wu, Y., Jeans, J., Suggett, D. J., Finkel, Z. V., and Campbell, D. A.: Large centric diatoms allocate more cellular nitrogen to photosynthesis to counter slower RUBISCO turnover rates, Front. Mar. Sci., 1, doi:10.3389/fmars.2014.00068, 2014a.

Wu, Y., Campbell, D. A., Irwin, A. J., Suggett, D. J., and Finkel, Z. V.: Ocean acidification enhances the growth rate of larger diatoms, Limnol. Oceanogr., 59, 1027–1034, doi:10.4319/lo.2014.59.3.1027, 2014b.

Xu, J., Glibert, P. M., Liu, H., Yin, K., Yuan, X., Chen, M., and Harrison, P. J.: Nitrogen sources and rates of phytoplankton uptake in different regions of Hong Kong waters in summer, Estuar. Coast., 35, 559–571, doi:10.1007/s12237-011-9456-9, 2012.

Young, J. N., Goldman, J. A. L., Kranz, S. A., Tortell, P. D., and Morel, F. M. M.: Slow carboxylation of Rubisco constrains the rate of carbon fixation during Antarctic phytoplankton blooms, New Phytol., 205, 172–181, doi:10.1111/nph.13021, 2015.

Zorz, J. K., Allanach, J. R., Murphy, C. D., Roodvoets, M. S., Campbell, D. A., and Cockshutt, A. M.: The RUBISCO to photosystem II ratio limits the maximum photosynthetic rate in picocyanobacteria, Life, 5, 403–417, doi:10.3390/life5010403, 2015.

BGD
12, 16645–16672, 2015

Table 1. Carbon per cell (pg cell^{-1}), mass C : N ratio, and cellular contents of Chlorophyll *a* (pg cell^{-1}), total protein (pg cell^{-1}), Photosystem II PsbA subunit (attomoles cell^{-1}) and RUBISCO large subunit (RbcL, attomoles cell^{-1}) of *T. pseudonana* and *T. punctigera* under low (LN) and high nitrogen media (HN) across three levels of growth light. The values are presented as mean ± SD (n = 3 or 4); bold numbers show significant differences of cultures from LN and HN conditions ($p < 0.05$).

Strains	Growth light (μmol photons m^{-2} s^{-1})	Media N (μM)	Carbon (pg cell^{-1})	C : N	Chl *a* (pg cell^{-1})	Total protein (pg cell^{-1})	PsbA (attomoles cell^{-1})	RbcL (attomoles cell^{-1})
T. pseudonana	30	55	**10.5 ± 0.52**	6.25 ± 0.20	0.25 ± 0.03	**7.12 ± 0.65**	**0.73 ± 0.08**	**21.2 ± 0.91**
		550	**8.29 ± 0.84**	5.89 ± 0.50	0.27 ± 0.07	**4.88 ± 0.73**	**0.30 ± 0.04**	**7.23 ± 0.92**
	180	55	9.25 ± 2.00	6.41 ± 0.12	0.20 ± 0.04	4.49 ± 0.41	0.43 ± 0.03	8.68 ± 1.44
		550	8.09 ± 0.48	6.42 ± 0.32	0.13 ± 0.03	4.61 ± 0.23	0.33 ± 0.07	8.30 ± 1.45
	380	55	8.91 ± 1.41	7.67 ± 0.52	0.08 ± 0.02	4.31 ± 1.28	0.40 ± 0.07	8.25 ± 1.52
		550	8.71 ± 0.87	6.34 ± 0.87	0.09 ± 0.01	4.64 ± 0.37	0.34 ± 0.05	10.0 ± 2.55
T. punctigera	30	55	**5669 ± 560**	5.30 ± 0.64	142 ± 37.6	4424 ± 1221	246 ± 50.7	**9578 ± 5547**
		550	**7675 ± 430**	4.82 ± 0.32	115 ± 5.31	5703 ± 893	230 ± 64.2	**3524 ± 777**
	90	55	6752 ± 434	7.61 ± 2.10	83.5 ± 21.3	3992 ± 1192	215 ± 103	**5178 ± 2128**
		550	6921 ± 186	5.24 ± 0.50	79.1 ± 24.1	4475 ± 778	208 ± 44.6	**3138 ± 530**
	180	55	8281 ± 1421	**9.28 ± 1.88**	59.4 ± 28.5	**4225 ± 54.3**	206 ± 82.3	**6977 ± 3219**
		550	7160 ± 1565	**5.20 ± 0.59**	58.3 ± 14.8	**3503 ± 430**	168 ± 60.8	**2657 ± 420**

BGD
12, 16645–16672, 2015

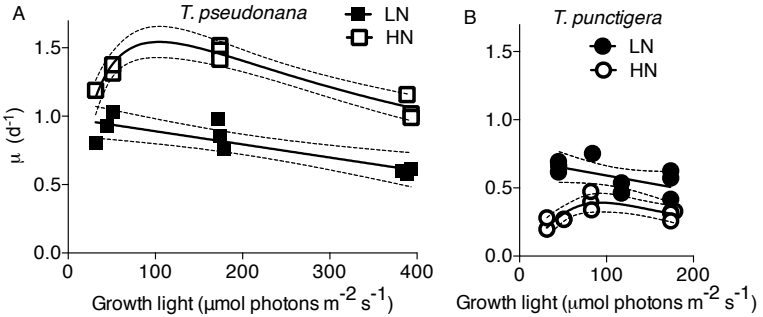

Figure 1. Growth rate (μ, d^{-1}) vs. culture growth light (μmol photons m^{-2} s^{-1}) of the small diatom **(a)** *Thalassiosira pseudonana* and **(b)** large diatom *Thalassiosira punctigera* under low (LN, filled symbols) and high nitrogen media (HN, open symbols). Solid lines: light response curves (Eilers and Peeters, 1988; Peeters and Eilers, 1978) or linear regressions; thin dotted lines show 95 % confidence intervals on the fitted curves.

BGD
12, 16645–16672, 2015

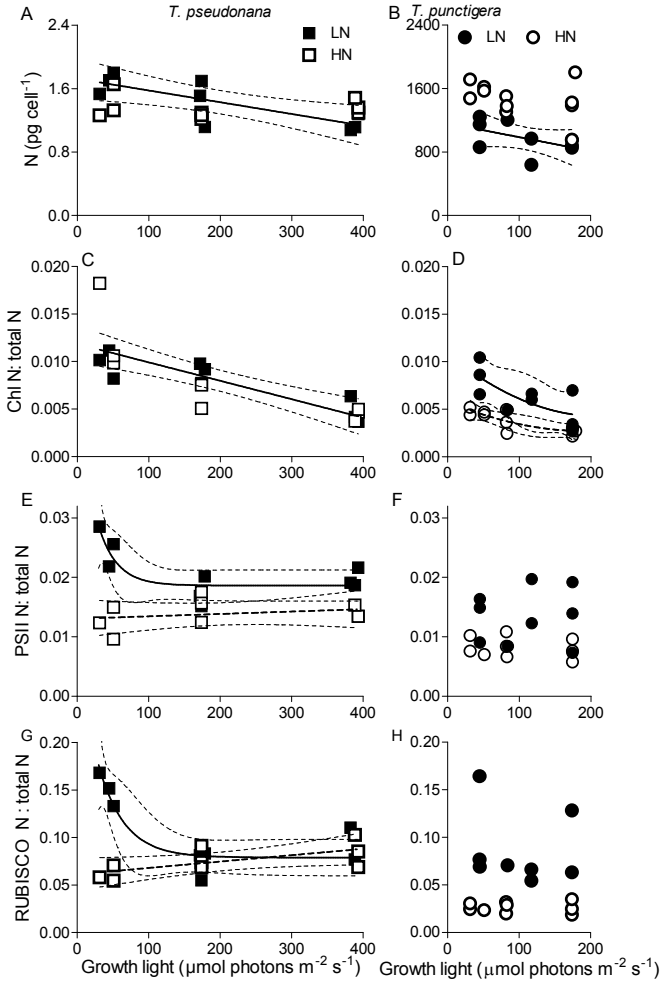

BGD
12, 16645–16672, 2015

RUBISCO allocations and function in *Thalassiosira*

G. Li and D. A. Campbell

Figure 2. Nitrogen per cell (pg cell^{-1}) vs. culture growth light (µmol photons m^{-2} s^{-1}) of **(a)** *T. pseudonana* and **(b)** *T. punctigera* under low (LN, filled symbols) and high nitrogen media (HN, open symbols). Solid line in panel **(a)**: linear regression for pooled growth light response for *T. pseudonana* from LN and HN conditions. Solid line in panel **(b)**: linear regression for growth light response for *T. punctigera* from LN condition only; thin dotted lines show 95 % confidence intervals on the fitted curves. Molar fraction of nitrogen allocated to Chlorophyll *a* relative to total cellular nitrogen (Chl *a* N : total N) vs. culture growth light (µmol photons m^{-2} s^{-1}) of **(c)** *T. pseudonana* and **(d)** *T. punctigera*. Solid line in panel **(c)**: linear regression for pooled growth light response for *T. pseudonana* from LN and HN. Lines in panel **(d)**: polynomial curves for *T. punctigera* from LN (solid) and HN (dashed). Molar Photosystem nitrogen to total nitrogen ratio (PSII N : total N) vs. culture growth light (µmol photons m^{-2} s^{-1}) of **(e)** *T. pseudonana* and **(f)** *T. punctigera*. Lines in panel **(e)**: exponential decay for *T. pseudonana* from LN (solid) or linear regression from HN (dashed). Molar RUBISCO N : total N ratio vs. culture growth light (µmol photons m^{-2} s^{-1}) of **(g)** *T. pseudonana* and **(h)** *T. punctigera*. Lines in panel **(g)**: exponential decay for *T. pseudonana* from LN (solid) and linear regression from HN (dashed).

BGD
12, 16645–16672, 2015

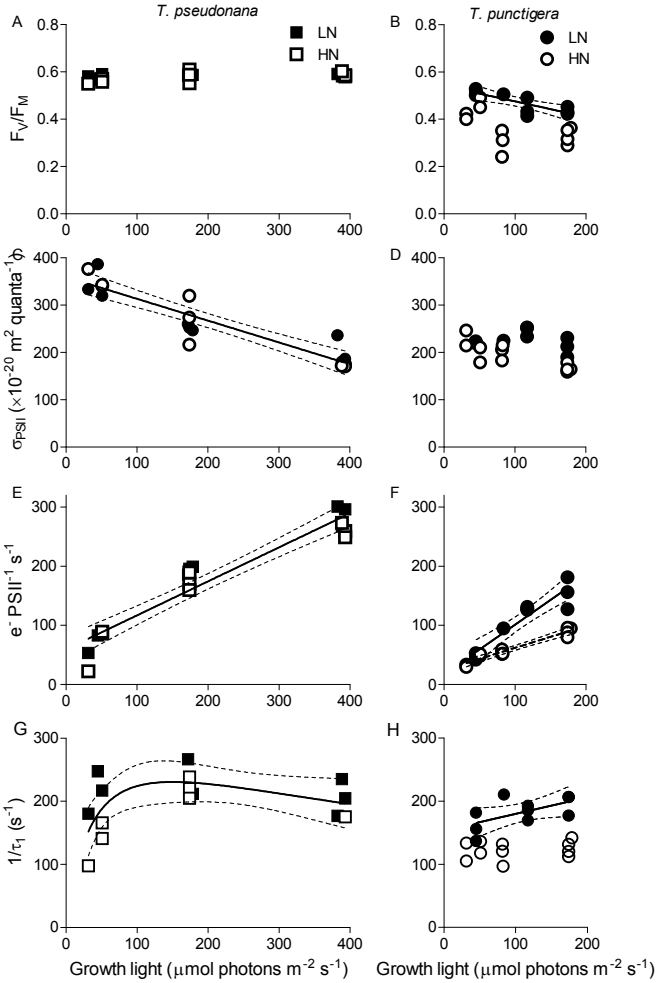

BGD
12, 16645–16672, 2015

RUBISCO allocations and function in *Thalassiosira*

G. Li and D. A. Campbell

Figure 3. Maximum Photosystem II photochemical quantum yield (F_V/F_M) vs. culture growth light (µmol photons m^{-2} s^{-1}) of **(a)** *T. pseudonana* and **(b)** *T. punctigera* under low (LN, filled symbols) and high nitrogen media (HN, open symbols). Solid line in panel **(b)**: linear regression for growth light response for *T. punctigera* from LN condition; thin dotted lines show 95 % confidence intervals on the fitted curves.Functional absorption cross-section for PSII photochemistry (σ_{PSII}, 10^{-20} m^2 quanta^{-1}) vs. growth light (µmol photons m^{-2} s^{-1}) of **(c)** *T. pseudonana* and **(d)** *T. punctigera*. Solid line in panel **(c)**: linear regression for pooled growth light response for *T. pseudonana* from LN and HN conditions. Electron transfer rate (e^- $PSII^{-1}$ s^{-1}) vs. growth light (µmol photons m^{-2} s^{-1}) of **(e)** *T. pseudonana* and **(f)** *T. punctigera*. Solid line in panel **(e)**: linear regression for pooled growth light response for *T. pseudonana* from LN and HN conditions. Lines in panel **(f)**: linear regressions for growth light response for *T. punctigera* from LN (solid) and HN (dashed) conditions. Slow decay lifetime (τ_1, µs) of chlorophyll fluorescence vs. culture growth light (µmol photons m^{-2} s^{-1}) of **(g)** *T. pseudonana* and **(h)** *T. punctigera*. Solid line in panel **(g)**: light response curve (Eilers and Peeters, 1988) for pooled τ_1 from LN and HN conditions. Solid line in panel **(h)**: linear regression for growth light response for *T. punctigera* from LN condition.

BGD
12, 16645–16672, 2015

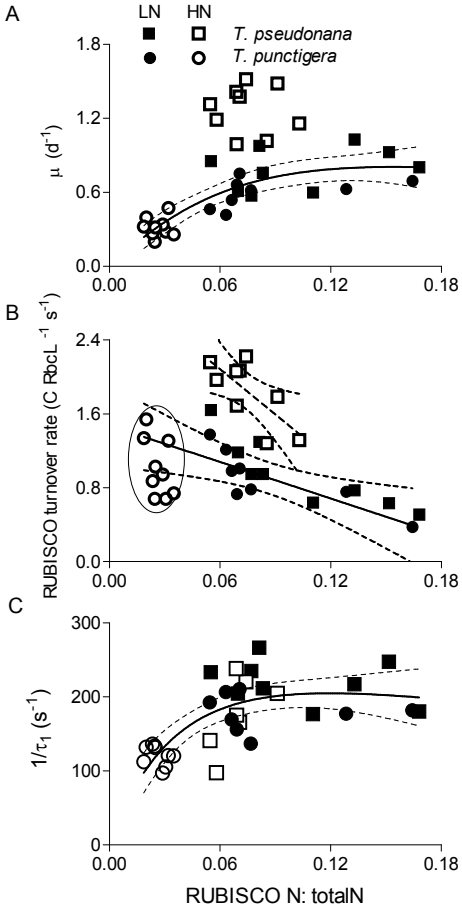

BGD
12, 16645–16672, 2015

RUBISCO allocations and function in *Thalassiosira*

G. Li and D. A. Campbell

Figure 4. (a) Growth rate (μ, d^{-1}) vs. molar RUBISCO N to total cellular N ratio (RUBISCO N : total N) of *T. pseudonana* (squares) and *T. punctigera* (circles) under low (LN, filled symbols) and high nitrogen media (HN, open symbols). A common saturating function (Eilers and Peeters, 1988) was fit to pooled data points, except *T. pseudonana* HN (open squares); thin dotted lines: 95 % confidence intervals on the fitted curves. **(b)** Apparent RUBISCO turnover rate (C Rbcl^{-1} s^{-1}) vs. RUBISCO N : total N of *T. pseudonana* and *T. punctigera*. Solid line: linear regression of pooled C Rbcl^{-1} s^{-1} vs. RUBISCO N : total N for *T. pseudonana* from LN condition and *T. punctigera* from LN and HN conditions. Oval outlines *T. punctigera* HN measures, which were included in the pooled regression. Dashed line shows separate regression for *T. pseudonana* HN (open squares). **(c)** $1/\tau_1$ (s^{-1}), the rate of electron transport away from PSII, vs. RUBISCO N : total N of *T. pseudonana* and *T. punctigera*. Solid line: the best response curve fitted with (Eilers and Peeters, 1988; Peeters and Eilers, 1978).

BGD
12, 16645–16672, 2015

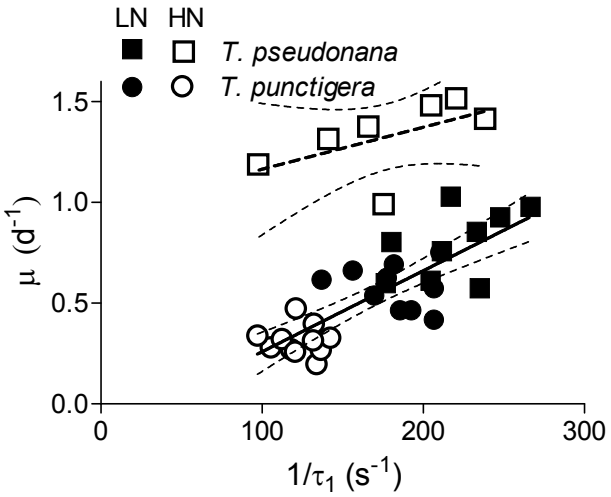

Figure 5. Growth rate (μ, d^{-1}) vs. $1/\tau_1$ (s^{-1}), the rate of electron transport away from PSII of *T. pseudonana* (squares) and *T. punctigera* (circles) under low (LN, filled symbols) and high nitrogen media (HN, open symbols). Solid line: linear regression of pooled μ vs. $1/\tau_1$ for *T. pseudonana* from LN condition and *T. punctigera* from LN and HN conditions. Dashed line: linear regression for *T. pseudonana* from HN only; thin dotted lines: 95 % confidence intervals on the fitted curves.

BGD
12, 16645–16672, 2015